Journal of Polymer Science and Engineering (2022) Volume 5 Issue 1
doi: 10.24294/jpse.v5i1.431

ORIGINAL RESEARCH ARTICLE

Effect of sewage sludge ash filler on mode I and mode II interlaminar fracture toughness of S-glass/epoxy composites

Mohamad Alsaadi[1,2,*], Ahmet Erkliğ[2]

[1] *Materials Engineering Department, University of Technology, Baghdad 10066, Iraq*

[2] *Faculty of Engineering, Mechanical Engineering Department, Gaziantep University, Gaziantep 27310, Turkey*

*** Corresponding author:** Mohamad Alsaadi, mohamad.alsaadi@mail2.gantep.edu.tr

ABSTRACT

In this study, the influence of sewage sludge ash (SSA) waste particle contents on the mechanical properties and interlaminar fracture toughness for mode I and mode II delamination of S-glass fiber-reinforced epoxy composites was investigated. Composite laminate specimens for tensile, flexural double-cantilever beam (DCB), and end-notched fracture (ENF) tests were prepared and tested according to ASTM standards with 5, 10, 15, and 20 wt% SSA-filled S-glass/epoxy composites. Property improvement reasons were explained based on optical and scanning electron microscopy. The highest improvement in tensile and flexural strength was obtained with a 10 wt% content of SSA. The highest mode I and mode II interlaminar fracture toughness's were obtained with 15 wt% content of SSA. The mode I and mode II interlaminar fracture toughness improved by 33% and 63.6%, respectively, compared to the composite without SSA.

Keywords: SSA; glass fiber; epoxy; mechanical properties; fracture toughness; delamination

ARTICLE INFO

Received: 6 July 2022
Accepted: 11 August 2022
Available online: 6 September 2022

1. Introduction

G Glass fiber-reinforced polymer (GFRP) composites have superior properties such as high stiffness, strength, thermal stability, and resistance to chemical hurt[1]. However, GFRP is often limited in use in automobiles, medical applications, aviation, construction, and military applications due to its poor resistance to interlaminar fracture[2,3]. This issue may be ascribed to the lack of fiber reinforcement oriented in the laminate depth for effective transverse of the applied force that can be circumvented by Z-fiber stitching or pinning other fibers to join layers[4–6]. However, the tensile properties of composites are reduced by this technique and require other manufacturing procedures[7]. Therefore, the most common polymer used in these laminates is epoxy. To date, two procedures have been used to improve interlaminar fracture toughness. First, researchers have used special structures of epoxy, like dendritic hyperbranched polymers; nevertheless, the interlaminar fracture resistance needs more improving[8]. The other method, epoxy matrix, is toughened by incorporating additional constituents, thermoplastics[9] and rubber particles[10]. For thermoplastics, epoxy viscosity is extremely elevated after high-molecular-weight thermoplastics are mixed with the epoxy resin, which causes difficulties in composite laminate fabrication. Rubber particles are the same as thermoplastics, and even though the

interlaminar fracture toughness is usually elevated due to the phase-separated structure in blends, the modulus and strength are dropped.

In recent years, particular attention has been paid to rigid inorganic particulate fillers, especially nanoparticles like nanoclay, nanosilica, carbon nanotubes, and nano-alumina[11–20], due to their improvement in the interlaminar fracture toughness of fiber-reinforced epoxy resin in composites. Jen et al.[21] improved PEEK/AS-4 composite strength by 12% with the addition of 1 wt% of nanosilica particles. Wang et al.[22] examined nano-whiskers to increase mode I interlaminar toughness of the composite from 140 J/m2 to 220 J/m^2. Wang et al.[23] used Al_2O_3 micro-particles to raise flexural strength, impact strength, and mode II interlaminar toughness by 16%, 37%, and 50.0%, respectively, for carbon fiber-reinforced epoxy composites. Some researchers have used SSA as an industrial waste filler to improve some mechanical properties like tensile and flexural strength of the composites used for construction applications such as bricks and tiles, as a raw material for cement production, and as aggregates for concrete and mortar[24]. Hence, compared with the previously stated methods, the addition of rigid particles may increase the mode I and mode II interlaminar toughness without losing other mechanical properties. Thus, it is more appropriate to study the effects of micro- and nano-particle content, especially waste particulate filler, on the property and mechanism of interlaminar fracture toughness to be more clarified.

Population and plant growth increase wastewater all over the world. Sewage sludge ash is generated during the combustion of dewatered SSA in a burner. SSA is stored and can be used as a filler material. One of the major environmental issues is the elimination of some materials that can provide economical and sustainable solutions. SSA contains compounds that are not harmful to the environment, like oxides. The annual amount of SSA is about 3.5 billion m^3 in Turkey[25]. When 4% of this amount is considered waste sedimentary, 140 million tons of SSA potential are available in Turkey. A sludge incineration system was first developed in Gaziantep[26]. The system generates electricity by burning approximately 150 tons of SSA per day. About 15 tons of ash remain at the end of combustion. When the established mechanism is thought of as a recycling system, the use of remaining ash increases the value of the mechanism, and the use of ash can also be regarded as a versatile earning method due to its environmental problems. The application of the SSA to the fabric and epoxy composite materials was examined in the present study.

Based on the above studies, many of these studies are related to mechanical properties and interlaminar toughness using a variety of micro- and nano-particle-filled composites. To the best knowledge of the authors, researchers in the literature do not adequately investigate the influence of SSA filler content on the interlaminar fracture toughness of GFRP. The focus of this study was to investigate the effect of SSA content on the tensile strength, flexural properties, and interlaminar fracture toughness for mode I and mode II deformation of glass fiber-reinforced epoxy (GRE) composites. In addition to investigating the interlaminar fracture behavior of each composite laminate, the forms of failure and deformation were examined using scanning electron and optical microscopes in order to present the toughening mechanism of each composite laminate.

2. Material properties and experimental procedures

2.1. Materials

To prepare the particulate-filled composite laminates, epoxy (MOMENTIVE-MGS L285) with hardener (MOMENTIVE-MGS H285) were blended in a stoichiometric weight ratio of 100/40. Woven plain S-glass fibers with areal density of 200 g/m^2 were used as reinforcement in the laminated composites. Production materials were provided by DOST Chemical Industrial Raw Materials Industry, Turkey. The SSA filler was supplied by Çatalağzı Power Plant, Şahinbey Belediyesi, Gaziantep, Turkey. The particle size was measured

approximately 1–35 µm for grinded and garbled SSA. The bulk density of SSA was measured as 0.72 gr/cm^3, and its chemical compositions are given in **Table 1**.

Table 1. Chemical compositions of the filler materials.

Filler	Chemical formula/composition (wt %)
Sewage sludge ash	P_2O_5 (23.56), CaO (19.58), SiO_2 (16.6), SO_3 (8.53), MgO (8.22), Fe_2O_3 (7.46), Al_2O_3 (5.73), K_2O (4.87), ZnO (2.09), TiO_2 (1.08), Cl (0.54), Na_2O (0.44), Cr_2O_3 (0.24), BaO (0.21), CuO (0.19), MnO_2 (0.18).

2.2. Composites production and samples preparation

The grinded of SSA filler was garbled by sieving to get fine particles in the range of 1–35 µm. The composites were prepared by adding SSA particles in epoxy resin with four different contents 5, 10, 15 and 20 wt%. The measured quantity of the SSA was added gradually in the epoxy resin and mixed it evenly by using a mechanical stirrer with a constant speed of 750 RPM for 25 min in order to obtain a homogeneous mixture. Then hardener was added to the mixture for quick setting of laminate composite. Laminated fabrics were manufactured by the application of the resin mixture to the S-glass fibers layer by layer at room temperature (25 °C). This process is repeated till all the 16 layers were placed. A heat-resistant Teflon film with thickness of 12 µm was inserted at mid-plane along one edge of the laminate during hand lay-up process in order to introduce a starter crack for double-cantilever beam (DCB) and end-notched flexure (ENF) specimens. Then, modified laminated fabrics with dimensions of 240 mm × 300 mm were applied to 0.3 MPa pressure between two flat molds with 80 °C temperature for 1 h curing time. Afterward, laminate was cooled to the room temperature under the pressure (Process of laminate production is shown in **Figure 1**). After the production of composite laminates tensile, flexural, DCB and ENF specimens (**Figure 2**) were cut according to ASTM standards.

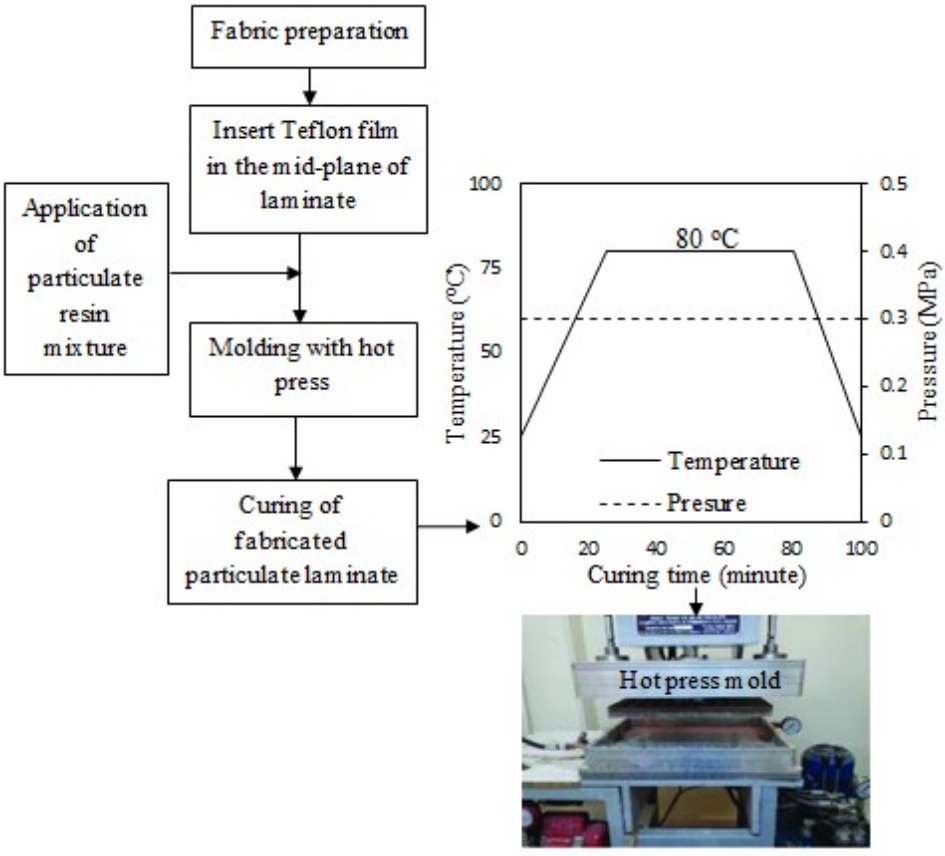

Figure 1. Production process and unit.

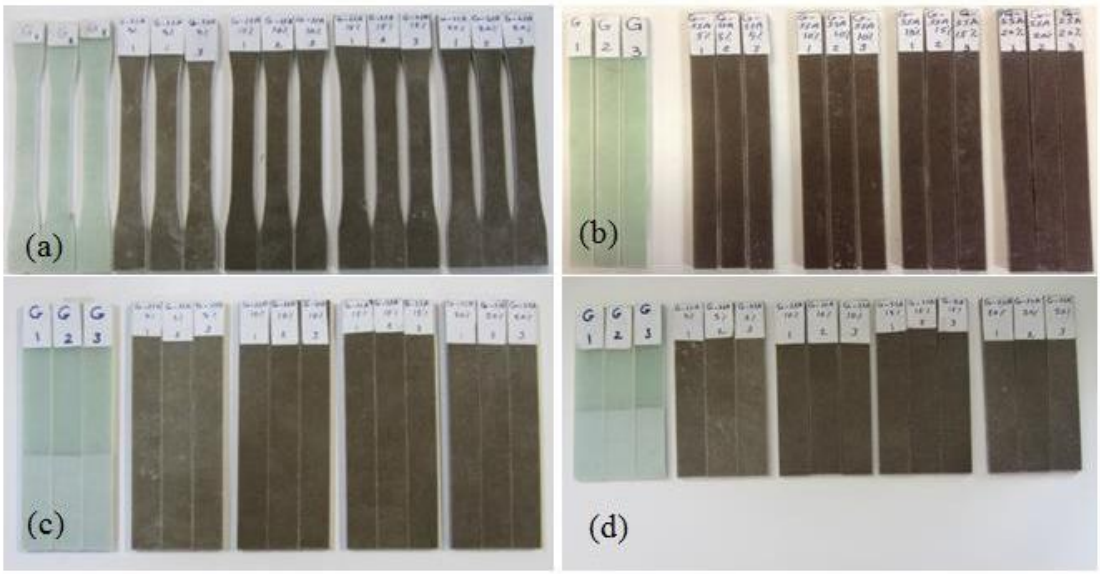

Figure 2. Specimens of SSA-GRE composites for: **(a)** tensile; **(b)** flexural; **(c)** DCB; **(d)** ENF tests.

2.3. Mode I testing

Strain energy release rate (G) represents the resistance to delamination growth, which the interlaminar fracture toughness is a measured value for the critical energy release rate (GC). The mode I interlaminar fracture toughness (GIC) of the GRE and the SSA-GRE composites were evaluated using the DCB test according to the ASTM D 5528 standard[27]. The specimens of DCB test were cut in the dimensions of 165 mm × 20 mm. Aluminum loading blocks measuring 20 mm × 25 mm × 12 mm with a loading hole of 6 mm diameter were stuck to each side on the cracked end of DCB specimens by using Araldite 2014 adhesive. The pre-crack length (a_o) was 50 mm according to the inserted Teflon film. **Figure 3** shows the configuration of DCB test specimen and a picture for specimen during testing. The crosshead displacement in the DCB test was explained as crack opening displacement (COD) of the specimen. The crack propagation length were recorded using a digital camera. The crosshead speed of DCB tests was 5 mm/min in accordance with ASTM D 5528. The data of DCB test were recorded in term of P-COD and corresponding *P*-a values, which a and *P* refer to crack extension length and load applied at which the crack grows, respectively. The mode I interlaminar fracture toughness (GIC) is determined by using the general formula from linear elastic fracture mechanics[2]:

$$G_{IC} = \frac{P^2}{2b}\frac{\partial C}{\partial a} = \frac{P\delta}{2bC}\frac{\partial C}{\partial a} \quad (1)$$

where b is the specimen width, δ is the COD and C is the compliance. By differentiating the compliance C, which C is equal to δ/P, and substitution into Equation (1) to obtain[2,27–29](Equation (2)):

$$G_{IC} = \frac{3P\delta}{2ba} \quad (2)$$

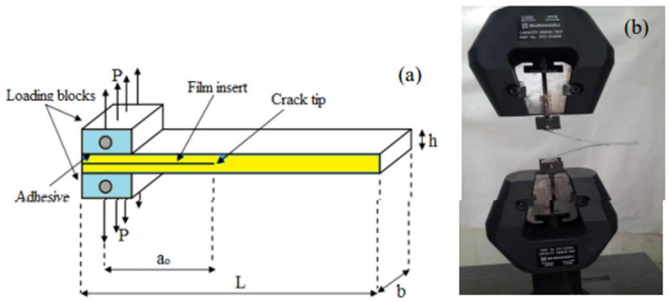

Figure 3. **(a)** Configuration of the DCB test specimen; **(b)** specimen under testing.

In reality, this expression overestimates G_{IC} values because the equation above is valid only for the perfectly built-in cantilever beam. In practice, the DCB is not perfectly built-in, therefore corrections are needed for shear deformation, rotation at the crack tip and large displacements. Some of these effects may be treated by correcting the crack length, that becomes slightly longer, a + |Δ|, where the crack length correction, Δ may be found by plotting cube root of the compliance, $C^{1/3}$, as a function of the crack extension length. The mode I interlaminar toughness now becomes[2,27–30] (Equation (3)):

$$G_{IC} = \frac{3P\delta}{2b(\alpha + |\Delta|)} \tag{3}$$

2.4. Mode II testing

The ENF test was conducted to determine the mode II interlaminar fracture toughness (G_{IIC}). The three-point bend fixture was used to perform this test with a span length of 76 mm[31]. The ENF specimen was prepared in 120 mm × 20 mm size. **Figure 4** shows the geometry of the ENF specimen and a picture for specimen during testing. The specimens were designed that (a/L) is 0.5 at the crack propagation. Controlling displacement was applied with a loading rate of 1 mm/min[28–30]. During the test the ENF specimen creates shear stress at the crack tip. When the crack propagation starts, the load suddenly dropped and the specimen failed. The direct beam theory was adopted for determining G_{IIC} using the equation below[28–33] (Equation (4)):

$$G_{IIC} = \frac{9P\delta a^2}{2b(2L^3 + 3a^3)} \tag{4}$$

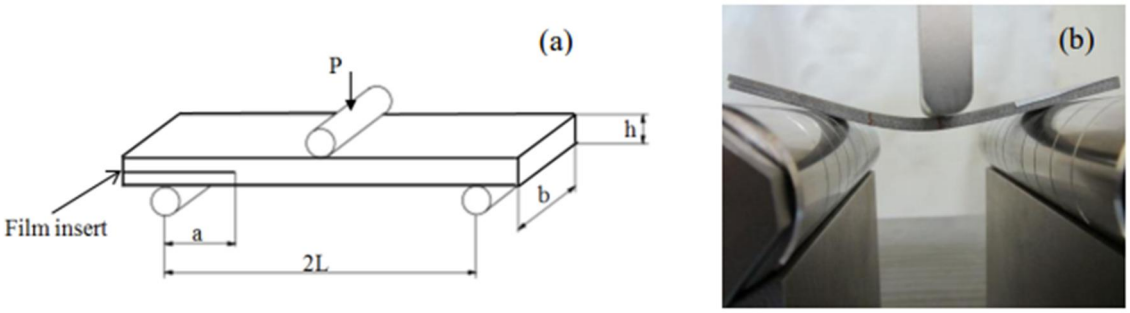

Figure 4. (a) Geometry of the ENF specimen; **(b)** specimen under testing.

3. Results and discussions

Tensile strength and flexural properties of GRE and SSA-GRE composites are given in **Table 2**, also detailed investigations are illustrated in **Figures 5** and **6**. As shown in **Figure 5**, the maximum tensile strength is 422 MPa at the SSA content of 10 wt% with maximum increment of 8.4%, compared with GRE composite. Hence, the composite tensile strength regularly increased with adding SSA up to 10 wt%, and then followed the trend of decreasing to reach 370 MPa at 20 wt% of SSA. The same behavior was observed for flexural strength versus SSA content. The highest enhancement of flexural strength was also obtained at SSA content of 10 wt% with maximum increment of 33.2 %. In general, all the specimens of the SSA-GRE composites have flexural strength higher than GRE composite. For example, the flexural strength increased from 410 MPa to 546 MPa when the SSA content changed from 0 wt% to 10 wt%, then further increasing SSA particles, the flexural strength reduced to 459 MPa.

Table 2. Mechanical properties of the composites.

Composite type	SSA content (wt%)	Tensile strength (MPa)	Flexural strength (MPa)	Failure strain (%)	Flexural modulus (MPa)
GRE	0	389 (± 09)	410 (± 11)	2.08 (± 0.05)	21.0 (± 0.32)
	5	391 (± 11)	501 (± 22)	2.41 (± 0.03)	21.6 (± 0.41)
SSA-GRE	10	422 (± 16)	546 (± 25)	2.55 (± 0.09)	21.7 (± 0.50)
	15	386 (± 14)	520 (± 09)	2.41 (± 0.04)	22.2 (± 0.35)
	20	370 (± 08)	459 (± 14)	2.35 (± 0.07)	20.9 (± 0.14)

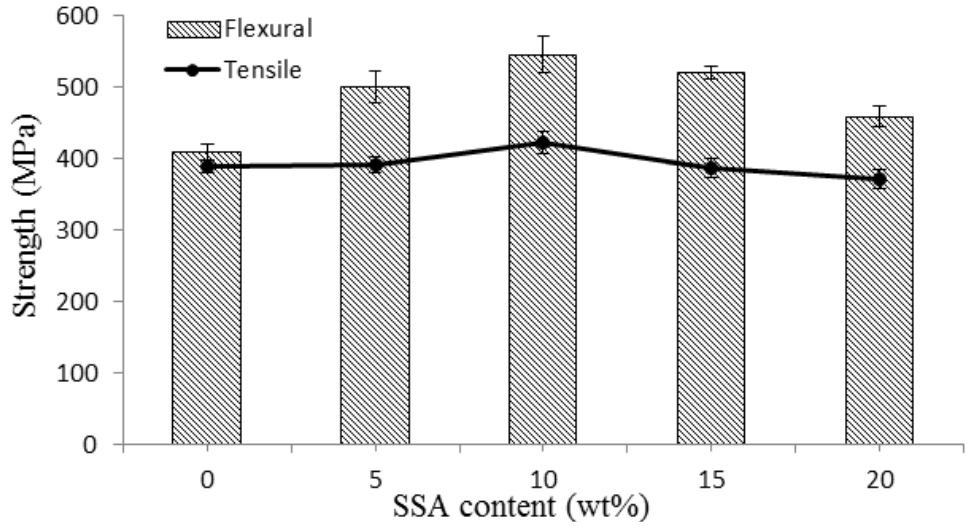

Figure 5. Tensile and flexural strength versus SSA content for the GRE and SSA-GRE composites.

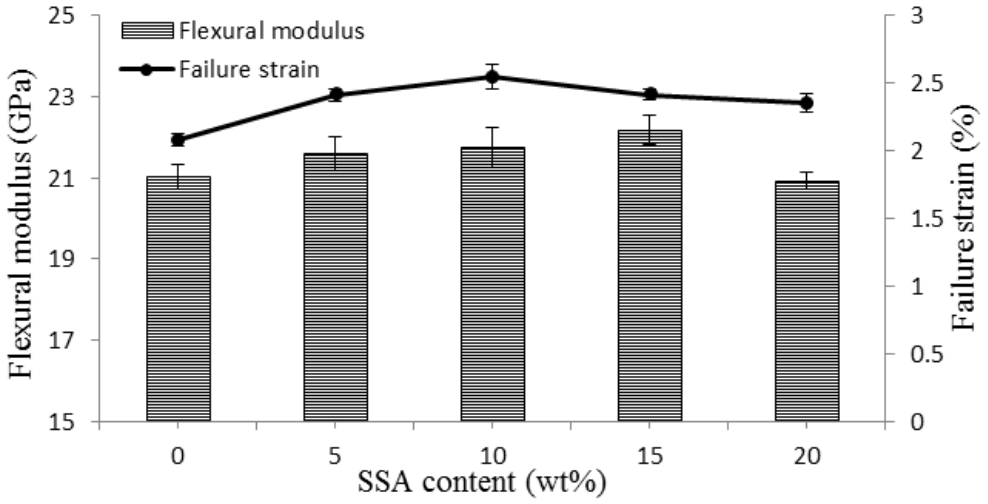

Figure 6. Flexural modulus and failure strain versus SSA content for the GRE and SSAGRE composites.

In principle, the failure strain values (**Figure 6**) of the GRE specimens moderately enhanced by adding SSA particles. Hence, the failure strain improved by 22.5% at SSA content of 10 wt%. Furthermore, the failure strain increased firstly from 2.08% for GRE composite to 2.55% and then reduced to 2.35% at 20 wt% of SSA, which perhaps due to the higher modulus of rigid inorganic SSA particles than that of the polymer matrix. The flexural modulus of SSA-GRE composites (**Figure 6**) was affected by inclusion of SSA, that the maximum modulus increased by 5.7% at SSA content of 15 wt%. While the flexural properties are degraded with thermoplastic filler addition, this strategy of using cheap industrial inorganic particles at least partly enhanced the mechanical properties. As a result of the tensile and flexural experiments, SSA particles, added in GRE composite, actually remarkably improved the flexural properties and tensile

strength. The drop of the strength values may be attributed to the particle aggregation when the SSA content more than 10 wt%, forming weaknesses in the composite.

3.2. Effect of SSA contents on mode I interlaminar toughness

Figure 7 shows the load-COD curves obtained by conducting DCB tests on specimens of GRE composite toughened by different SSA weight fractions. The figure shows that, the GRE and SSA-GRE composites exhibit a linear load-COD behavior up to the crack initiation point, afterward these curves exhibited non-linear crack growth behavior. Furthermore, the gap is small between the non-linear point and maximum load point. Besides, the maximum load point increased by the addition of SSA to GRE composite. However, the fracture behavior of DCB specimen was distinctly different after addition of SSA. Hence, the maximum load-COD of GRE is about 23 N-78 mm, while for SSA-GRE composites are about 27 N-72 mm, 28 N-74 mm, 34 N-69 mm and 32 N-68 mm, respectively when the SSA content changed from 5, 10, 15, to 20 wt%, as presented in **Table 3**.

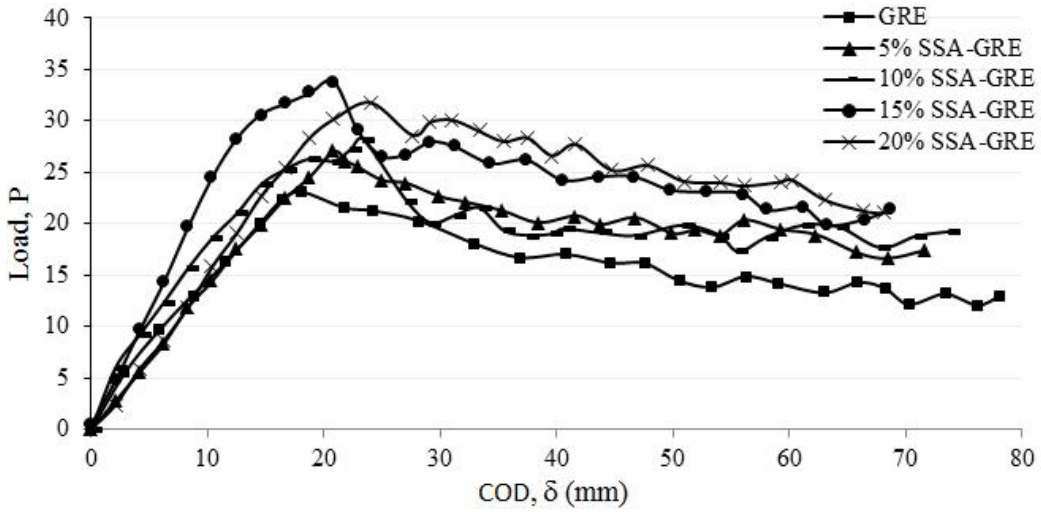

Figure 7. Load-COD curves of the DCB tests for the GRE and SSA-GRE composites.

Table 3. Mode I interlaminar fracture toughness properties of the composites.

Composite type	SSA content (wt%)	Maximum load (N)	Maximum COD (mm)	G_{IC}-Onest (J/m^2)	G_{IC}-Onest increment (%)	G_{IC}-Prop (J/m^2)	G_{IC}-Prop increment (%)
GRE	0	23.3 (± 1.7)	78.1 (± 3.9)	441 (± 18)	-	615 (± 27)	-
	5	26.9 (± 1.5)	17.7 (± 2.9)	445 (± 17)	0.9	147 (± 17)	4.2
SSA-GRE	10	28.2 (± 0.9)	17.7 (± 2.4)	520 (± 20)	17.9	116 (± 21)	10.2
	15	33.8 (± 2.1)	66.1 (± 1.8)	661 (± 36)	7.23	146 (± 19)	21.3
	20	31.5 (± 1.6)	11.3 (± 2.6)	564 (± 19)	.621	133 (± 28)	13.7

In details, when DCB test was conducted and the applied opening load reached near the maximum value, the delamination starts to propagate from the pre-crack tip (tip of the film insert) up to the delamination length reached 100 mm. Therefore, 9 steady state crack growth behavior was observed such that insignificant rise and decrease of load values (zigzag) are noticed with respect to the displacement. Furthermore, the fracture onset represents the maximum load-COD value, which refers to the changing from the linear to nonlinear behavior in the load-COD curve. During the delamination extension, the bridged fibers were cracked or peel-off from the epoxy matrix and the separation of the both sides of the specimen increased, which this behavior explains the higher values of propagation fracture toughness (G_{IC}Prop) than that of initiation fracture toughness (G_{IC}-Onset) values[33–36].

Resistance curves (R-curves) for the composites are presented in **Figure 8**. These curves demonstrate the variation of G_{IC} versus delamination length of the GRE and SSA-GRE composites. The values of G_{IC}-

Onset and G_{IC}-Prop were defined according to the ASTM D-5528 standards[27], that G_{IC}-Onset at the maximum load point and G_{IC}-Prop corresponding to the average propagation values after maximum G_{IC} value of the R-curves.

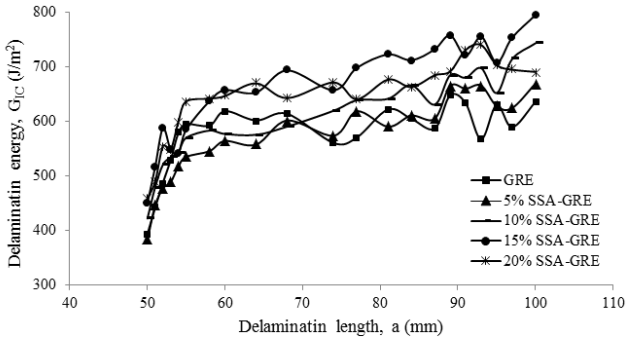

Figure 8. R-curves for the GRE and SSA-GRE composites.

As illustrated in **Figure 9**, G_{IC}-Onset and G_{IC}-Prop are enhanced with addition of SSA in GRE laminates. Hence, the G_{IC}-Onset of GRE composite was 441 J/m^2. When the SSA content increased from 5 wt% to 15 wt%, the G_{IC}-Onset increased from 445 J/m^2 to 586 J/m^2 to record increment from 0.9% to 32.9%, respectively compared with GRE composite. Same trend was noticed for the G_{IC}-Prop that for GRE composite was 615 J/m^2. When the SSA content increased from 5 wt% to 15 wt%, the G_{IC}- Prop increased from 641 J/m^2 to 745 J/m^2 to record increment from 4.2% to 21.3%, respectively compared with GRE composite. The slight drop in G_{IC} values after addition of SSA more than 15 wt% may be described to the negative effects of void content and particle aggregation on the adhesion strength between SSA particles and matrix, which they act as stress concentration points and weakened the composite[13,23].

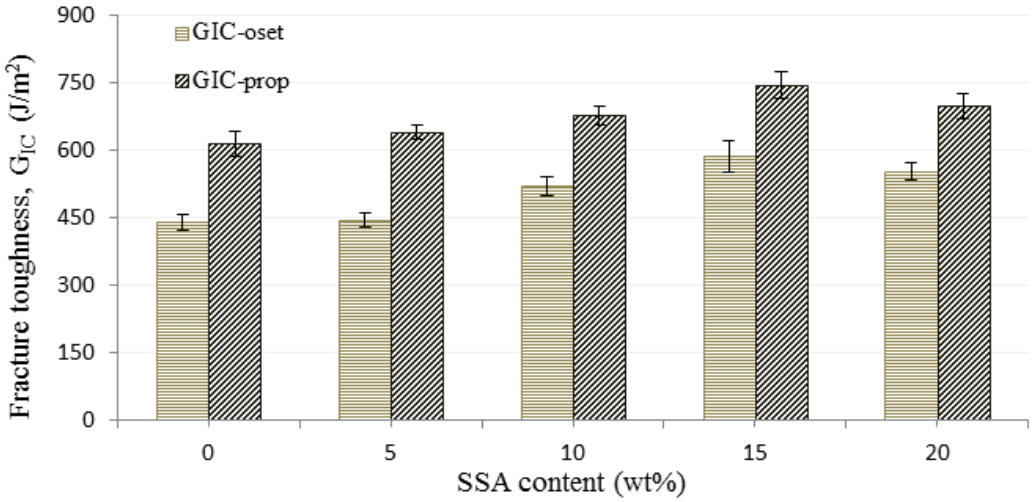

Figure 9. Comparison of mode I interlaminar toughness values for the GRE and SSA-GRE composites.

3.3. Mechanisms of mode I interlaminar toughness

Figure 10 depicts cross-section images of DCB specimens observed by optical microscope for the GRE and 15 wt% SSA-GRE composites. The cross-section images were selected at a place near the crack initiation point (**Figure 10(a,c)**) and the final stage of crack propagation (**Figure 10(b,d)**). For the GRE specimen, the interlayer crack is straight, as shown in **Figure 10(a)**. Moreover, some fiber bundles of GRE specimen are pulled and broken out during the crack propagation, as presented in **Figure 10(b)**. Hence, For the SSA-GRE specimen (**Figure 10(c,d)**), the interlayer crack is not straight (kinked crack path) and has rougher surface[2], therefore, the fracture area increased compared with GRE specimen. Accordingly, the crack propagation in SSAGRE specimen started later than that in the GRE specimen. As shown in **Figure**

11(a,c), the SEM images of the fracture surfaces show clearly the pulled of glass fibers from matrix for GRE composite. On the other hand, for SSA-GRE composites, SSA particles bonded with matrix and settled around the glass fibers (**Figure 11(b,d)**), these SEM micrographs were taken for the specimens of higher toughness at SSA content of 15 wt%. As observed in SEM images, the crack propagated through the SSA particles without creating particle/matrix debonding. This behavior indicates the chemical compatibility of SSA particle/epoxy system. Moreover, this good adhesion was reduced the interlayer region and would hinder the formation of a plastic zone. Accordingly, the onset and propagation interlaminar fracture toughness of mode I delamination reached optimum values when the SSA was 15 wt%, then follow the trend of decreasing because of particle aggregation works as a defect, that lead to weakened the adhesion force between SSA particle and matrix[23].

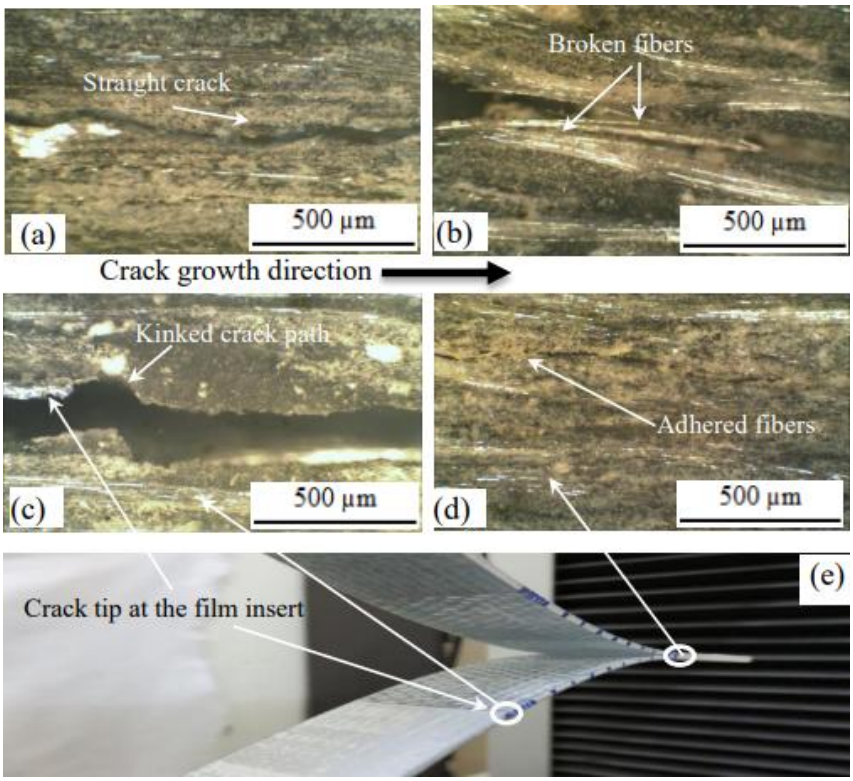

Figure 10. The optical microscope images of DCB specimen for GRE: **(a)** Crack near the film insert; **(b)** At the end of crack propagation, and for 15 wt% SSA GRE; **(c)** Crack near the film insert; **(d)** At the end of crack propagation; **(e)** The specimen.

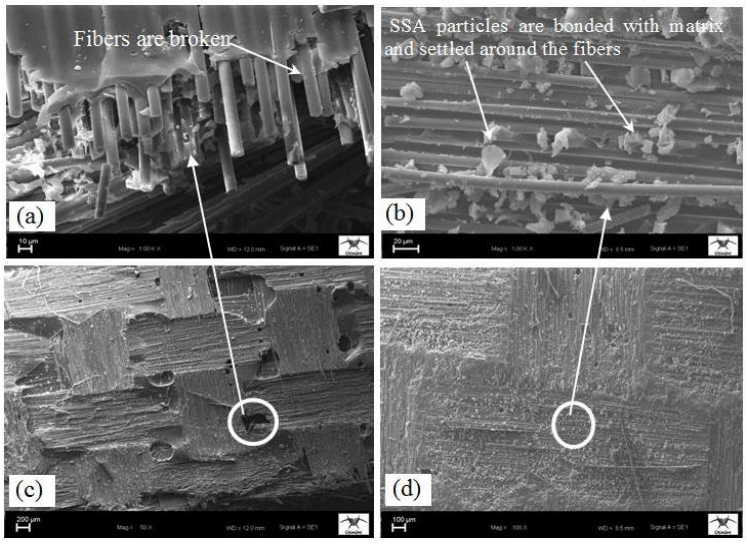

Figure 11. SEM micrographs of mode I fracture surfaces of DCB specimens for: **(a)** GRE; **(b)** 15 wt% SSA-GRE; **(c)** GRE; **(d)** 15 wt% SSA-GRE.

3.4. Effect of SSA contents on mode II interlaminar toughness

Figure 12 shows the representative load-displacement curves obtained by conducting ENF tests. As can be seen in figure, the GRE and SSA-GRE composites show a linear load–displacement behavior up to the point of crack initiation, afterwards load suddenly decreased and caused the unstable crack propagation and fracture. This behavior is affected by the brittle nature of epoxy resin. Moreover, there is a plateau at the highest load. Therefore, the crack propagation was delayed by SSA particles[23,29].

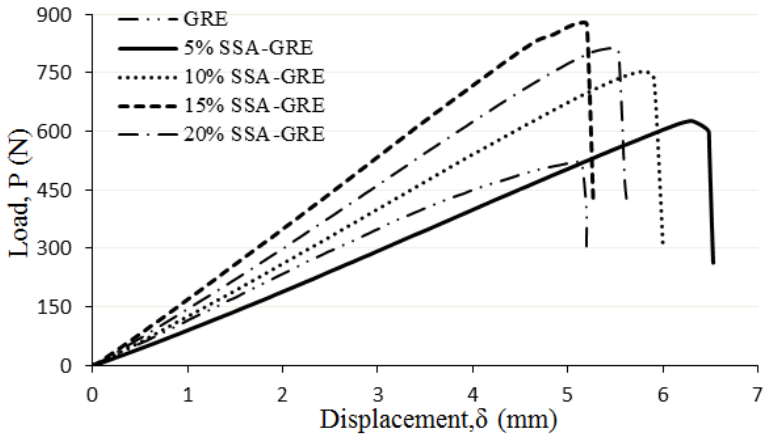

Figure 12. Load-displacement curves of the ENF tests for the GRE and SSA-GRE composites.

For the GRE composite, the maximum load and displacement values were about 522 N and 5.08 mm, respectively. On the other hand, after SSA addition, the maximum load increased gradually with increasing SSA content. Hence, the maximum load-displacement values for SSA-GRE composites were about 625 N-6.3 mm, 799 N-5.5 mm, 878 N-5.14 mm and 813 N-5.47 mm, when the SSA content changed from 5, 10, 15, to 20 wt%, respectively. The detailed results are given in **Table 4**.

Table 4. Mode II interlaminar fracture toughness properties of the composites.

Composite type	SSA content (wt%)	Maximum load (N)	Displacement at maximum load (mm)	Fracture toughness G_{IIC} (J/m^2)	G_{IIC} increment (%)
GRE	0	522 (± 22)	5.08 (± 0.12)	1720 (± 66)	-
SSA-GRE	5	625 (± 15)	6.30 (± 0.13)	2454 (± 52)	42.7
	10	799 (± 16)	5.50 (± 0.07)	2738 (± 69)	59.2
	15	878 (± 13)	5.14 (± 0.08)	2812 (± 37)	63.6
	20	813 (± 7)	5.47 (± 0.05)	2770 (± 39)	61.1

The G_{IIC} of the composites had the highest value of 2812 J/m^2 at SSA content of 15 wt% (**Figure 13**). Then G_{IIC} was dropped at SSA content of 20 wt%. Compared with that of GRE composite, G_{IIC} of the SSA-GRE composite increased by 42.7%, 59.2%, 63.6% and 61.1%, respectively.

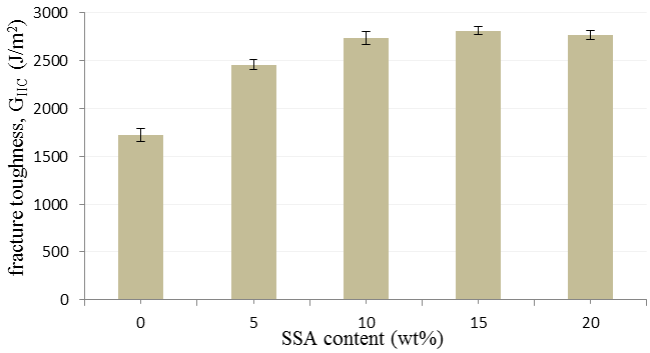

Figure 13. Mode II interlaminar fracture toughness for the GRE and SSA-GRE composites.

3.5. Mechanisms of mode II interlaminar toughness

The ENF specimen was applied to mode II loading creates maximum shear stress causes crack initiation and propagation in a form of crack moving from the crack tip at the film insert to mid-span of the specimen. The cross-section of the specimens was inspected by optical microscope for the GRE and SSA-GRE composites (**Figure 14(a,b)**) at a place near the crack tip point. As shown in **Figure 14(a)**, the glass fibers are exposed during crack propagation between the surface of the fabric material and the matrix, while **Figure 14(b)** illustrates the plastically deformed zones keep good adhesion for SSA particle/fiber/epoxy system. Chai[37,38] introduced similar procedure for presenting the plastic shear deformation, which is the main parameter in controlling mode II interlaminar toughness.

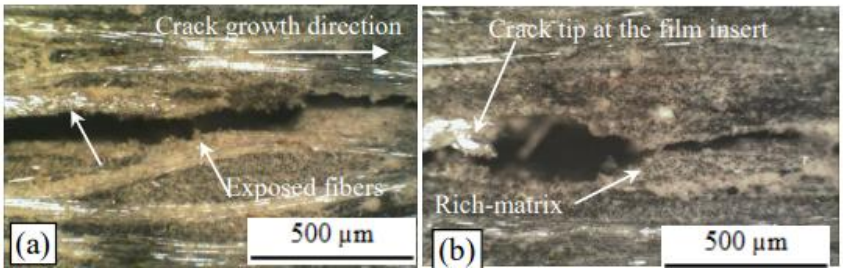

Figure 14. The optical microscope images for mode II specimen cross-section: **(a)** GRE; **(b)** 15 wt% SSA-GRE (Crack near the film insert).

Figure 15 demonstrates SEM images of the fracture surface for ENF specimens in order to clarify the mode II interlaminar toughness results. In general, the mode II fracture was brittle fracture. Nevertheless, the fracture surface was different after SSA addition at the ply of interlayer. As shown in the specimen fracture surfaces near the mid-span (**Figure 15(a,c)**) for the GRE composite, the fibers were pulled out and broken. On the other hand, as observed in SEM images (**Figure 15(b,d)**), the crack propagated through the particles without creating particle/matrix debonding. Moreover, hackles were observed on the fracture surface to provide significant toughening[2,37], this good adhesion was reduced the interlayer region and would hinder the formation of a plastic zone. The mode II interlaminar fracture toughness decreased when the SSA content was more than 15 wt%, because of the particle aggregation in the composite also.

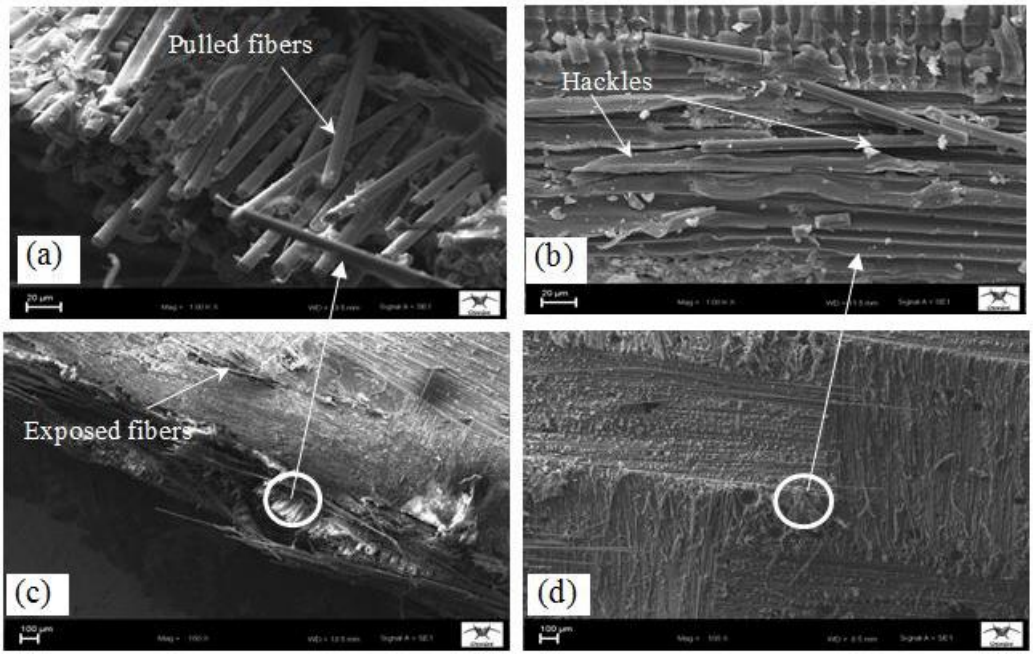

Figure 15. The micrographs of mode II interlaminar fracture surfaces in composites taken by SEM for: **(a)** GRE; **(b)** 15 wt% SSA-GRE; **(c)** GRE; **(d)** 15 wt% SSA-GRE.

4. Conclusions

The glass fabric/epoxy composite laminates containing micro-SSA particles were manufactured. The tensile, flexural, DCB, and ENF tests were carried out according to ASTM standards. The main conclusions from this work can be summarized as follows:

- The addition of SSA particles with four different weight fractions to glass fiber-reinforced composites significantly improved the tensile and flexural strength, flexural modulus, failure strain, and interlaminar fracture toughness for mode I and mode II delamination.
- The tensile strength, flexural strength, and flexural modulus reached their highest values at SSA content of 10, 10, and 15 wt%, with a maximum increment of 8.4%, 33.8%, and 5.7%, respectively.
- The load-COD curves of DCB specimens were distinctly different after particle addition. Hence, the maximum load point increased and positively affected mode I interlaminar toughness.
- The initiation and propagation of mode I interlaminar fracture toughness, G_{IC}-Onset and G_{IC}-Prop, were calculated from the R-curves of the DCB test, and their values were greatly increased by 32.9% and 21.3%, respectively, to reach maximum with a SSA content of 15 wt%.
- The mode II interlaminar fracture toughness values were calculated from the load-displacement data of the ENF test, and GIIC was optimum at a SSA content of 15 wt% with a maximum increment of 63.6%.
- The SEM and optical microscope images proved the improvement of mode I and mode II interlaminar fracture toughness, which can be mainly attributed to the high debonding resistance of the SSA particles in the matrix, and thus crack growth was delayed through specimens during the tests. This mechanism indicates the chemical compatibility of the SSA-GRE composite system.

Conflict of interest

The authors declare no conflict of interest.

References

1. Sathishkumar T, Satheeshkumar S, Naveen J. Glass fiber-reinforced polymer composites—A review. J*ournal of Reinforced Plastics and Composites* 2014; 33(13): 1258–1275. doi: 10.1177/0731684414530790
2. Srivastava VK, Hogg PJ. Damage performance of particles filled quasi-isotropic glass–fibre reinforced polyester resin composites. *Journal of Materials Science* 1998; 33: 1119–1128. doi: 10.1023/A:1004353020894
3. Salpekar SA, Raju IS, O'Brien TK. Strain-Energy-Release Rate Analysis of Delamination in a Tapered Laminate Subjected to Tension Load. *Journal of Composite Materials* 1991; 25(2): 118–141. doi: 10.1177/002199839102500201
4. Song MC, Sankar BV, Subhash G, et al. Analysis of mode I delamination of z-pinned composites using a non-dimensional analytical model. *Composites Part B: Engineering* 2012; 43(4): 1776–1784. doi: 10.1016/j.compositesb.2012.01.086
5. Mouritz AP, Koh TM. Re-evaluation of mode I bridging traction modelling for z-pinned laminates based on experimental analysis. *Composites Part B: Engineering* 2014; 56: 797–807. doi: 10.1016/j.compositesb.2013.09.016
6. Pegorin F, Pingkarawat K, Daynes S, et al. Influence of z-pin length on the delamination fracture toughness and fatigue resistance of pinned composites. *Composites Part B: Engineering* 2015; 78: 298–307. doi: 10.1016/j.compositesb.2015.03.093
7. Mouritz AP, Cox BN. A mechanistic approach to the properties of stitched laminates. *Composites Part A: Applied Science and Manufacturing* 2000; 31(1): 1–27. doi: 10.1016/S1359-835X(99)00056-1
8. Mezzenga R, Boogh L, Månson JA. A review of dendritic hyperbranched polymer as modifiers in epoxy composites. *Composites Science and Technology* 2001; 61(5): 787–795. doi: 10.1016/S0266-3538(01)00022-7
9. van der Heijden S, Daelemans L, De Schoenmaker B, et al. Interlaminar toughening of resin transfer moulded glass fibre epoxy laminates by polycaprolactone electrospun nanofibres. *Composites Science and Technology* 2014; 104: 66–73. doi: 10.1016/j.compscitech.2014.09.005
10. Dadfar MR, Ghadami F. Effect of rubber modification on fracture toughness properties of glass reinforced hot cured epoxy composites. *Materials & Design* 2013; 47: 16–20. doi: 10.1016/j.matdes.2012.12.035

11. Tang Y, Ye L, Zhang D, et al. Characterization of transverse tensile, interlaminar shear and interlaminate fracture in CF/EP laminates with 10wt% and 20wt% silica nanoparticles in matrix resins. *Composites Part A: Applied Science and Manufacturing* 2011; 42(12): 1943–1950. doi: 10.1016/j.compositesa.2011.08.019
12. Fan Z, Santare MH, Advani SG. Interlaminar shear strength of glass fiber reinforced epoxy composites enhanced with multi-walled carbon nanotubes. *Composites Part A: Applied Science and Manufacturing* 2008; 39(3): 540–554. doi: 10.1016/j.compositesa.2007.11.013
13. Zhu J, Imam A, Crane R, et al. Processing a glass fiber reinforced vinyl ester composite with nanotube enhancement of interlaminar shear strength. *Composites Science and Technology* 2007; 67(7–8): 1509–1517. doi: 10.1016/j.compscitech.2006.07.018
14. Wang K, Chen L, Wu J, et al. Epoxy Nanocomposites with Highly Exfoliated Clay: Mechanical Properties and Fracture Mechanisms. *Macromolecules* 2005; 38(3): 788–800. doi: 10.1021/ma048465n
15. Coleman JN, Khan U, Blau WJ, et al. Small but strong: A review of the mechanical properties of carbon nanotube–polymer composites. *Carbon* 2006; 44(9): 1624–1652. doi: 10.1016/j.carbon.2006.02.038
16. Shahid N, Villate RG, Barron AR. Chemically functionalized alumina nanoparticle effect on carbon fiber/epoxy composites. *Composites Science and Technology* 2005; 65(14): 2250–2258. doi: 10.1016/j.compscitech.2005.04.001
17. Gardea F, Lagoudas DC. Characterization of electrical and thermal properties of carbon nanotube/epoxy composites. *Composites Part B: Engineering* 2014; 56: 611–620. doi: 10.1016/j.compositesb.2013.08.032
18. Jiang Q, Wang X, Zhu Y, et al. Mechanical, electrical and thermal properties of aligned carbon nanotube/polyimide composites. *Composites Part B: Engineering* 2014; 56: 408–412. doi: 10.1016/j.compositesb.2013.08.064
19. Shiu SC, Tsai JL. Characterizing thermal and mechanical properties of graphene/epoxy nanocomposites. *Composites Part B: Engineering* 2014; 56: 691–697. doi: 10.1016/j.compositesb.2013.09.007
20. Chen Q, Wu W, Zhao Y, et al. Nano-epoxy resins containing electrospun carbon nanofibers and the resulting hybrid multi-scale composites. *Composites Part B: Engineering*. 2014; 58: 43–53. doi: 10.1016/j.compositesb.2013.10.048
21. Jen M, Tseng Y, Wu C. Manufacturing and mechanical response of nanocomposite laminates. *Composites Science and Technology* 2005; 65(5): 775–779. doi: 10.1016/j.compscitech.2004.10.010
22. Wang WX, Takao Y, Matsubara T, Kim HS. Improvement of the interlaminar fracture toughness of composite laminates by whisker reinforced interlamination. *Composites Science and Technology* 2002; 62(6): 767–774. doi: 10.1016/S0266-3538(02)00052-0
23. Wang Z, Huang X, Bai L, et al. Effect of micro-Al_2O_3 contents on mechanical property of carbon fiber reinforced epoxy matrix composites. *Composites Part B: Engineering* 2016; 91: 392–398. doi: 10.1016/j.compositesb.2016.01.052
24. Smol M, Kulczycka J, Henclik A, et al. The possible use of sewage sludge ash (SSA) in the construction industry as a way towards a circular economy. *Journal of Cleaner Production* 2015; 95: 45–54. doi: 10.1016/j.jclepro.2015.02.051
25. Turkish Statistical Institute. *Municipals Waste Water Statistics*. Turkish Statistical Institute; 2010.
26. Kütük MA, Aksoy M. A case study on sewage sludge incineration plant: GASKI. In: Proceedings of the Second International Conference on Water, Energy and the Environment; 21–24 September 2013; Kusadası, Turkey. pp. 21–24.
27. ASTM D5528-94A: Standard test method for Mode I interlaminar fracture toughness of unidirectional fiber-reinforced polymer matrix composites. Available online: https://standards.iteh.ai/catalog/standards/astm/c5f96a21-fd02-4f31-8126-50f14521e4d0/astm-d5528-94a (accessed on 2 February 2022).
28. Albertsen H, Ivens J, Peters P, Wevers M, Verpoest I. Interlaminar fracture toughness of CFRP influenced by fibre surface treatment: Part 1. Experimental results. *Composites Science and Technology* 1995; 54(2): 133–145. doi: 10.1016/0266-3538(95)00048-8
29. Tugrul Seyhan A, Tanoglu M, Schulte K. Mode I and mode II fracture toughness of E-glass non-crimp fabric/carbon nanotube (CNT) modified polymer based composites. *Engineering Fracture Mechanics* 2008; 75(18): 5151–5162. doi: 10.1016/j.engfracmech.2008.08.003
30. Dharmawan F, Simpson G, Herszberg I, et al. Mixed mode fracture toughness of GFRP composites. Composite Structures. 2006; 75(1–4): 328–338. doi: 10.1016/j.compstruct.2006.04.020
31. Carlsson LA, Gillespie JW, Pipes RB. On the Analysis and Design of the End Notched Flexure (ENF) Specimen for Mode II Testing. *Journal of Composite Materials* 1986; 20(6): 594–604. doi: 10.1177/002199838602000606
32. Lee JJ, Lim JO, Huh JS. Mode II interlaminar fracture behavior of carbon bead-filled epoxy/glass fiber hybrid composite. *Polymer Composites* 2000; 21(2): 343–352. doi: 10.1002/pc.10191
33. Srivastava VK, Hogg PJ. Moisture effects on the toughness, mode-I and mode-II of particles filled quasi-isotropic glass-fiber reinforced polyester resin composites. *Journal of Materials Science* 1998; 33(5): 1129–1136. doi: 10.1023/A:1004305104964
34. Lee SM. Mode II delamination failure mechanisms of polymer matrix composites. *Journal of Materials Science* 1997; 32(5): 1287–1295. doi: 10.1023/A:1018552506085

35. Wang TW, Blum FD, Dharani LR. Effect of interfacial mobility on flexural strength and fracture toughness of glass/epoxy laminates. *Journal of Materials Science* 1999; 34: 4873–4882. doi: 10.1023/A:1004676214290
36. Stevanovic D, Kalyanasundaram S, Lowe A, Jar PY. Mode I and mode II delamination properties of glass/vinyl-ester composite toughened by particulate modified interlayers. *Composites Science and Technology* 2003; 63(13): 1949–1964. doi: 10.1016/S0266-3538(03)00162-3
37. Chai H. Observation of deformation and damage at the tip of cracks in adhesive bonds loaded in shear and assessment of a criterion for fracture. *International Journal of Fracture* 1993; 60(4): 311–326. doi: 10.1007/bf00034739
38. Chai H. Micromechanics of shear deformations in cracked bonded joints. *International Journal of Fracture* 1992; 58(3): 223–239. doi: 10.1007/bf00015617